Rojava Journal of Science and Technology

2026, VOL. 3, No 1, [61-80]

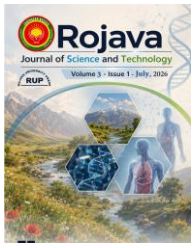

Microwave-Engineered Magnetite@ Bentonite@ Glutamic Acid Nanocomposite for Rapid and Efficient Removal of Remazol Red from Aqueous Systems

Maher Saif Al-Deen Ahmed[1], Haider Saify Nabiabad[2], Mohamad Elsayed Mahmoud[3], Rehab Mansour El-Sharkawy*[4]

[1] Dep. of Chemistry, Institute of Science and Modern Technology-Rojava University, Syria
[2] Dep. of Biotechnology, Institute of Science and Modern Technology-Rojava University, Syria
[3] Faculty of Science, Chemistry Department, Alexandria University, Egypt
[4] Faculty of Dentistry, Chemistry Department, Pharos University in Alexandria, Egypt

ABSTRACT

Objective: The creation of effective and sustainable adsorbents for wastewater contaminated with dyes is a significant environmental issue. Material and Methods: This research successfully developed a new magnetically recoverable nanocomposite, consisting of magnetite, bentonite, and glutamic acid (Fe_3O_4@BNT@GA), through a quick microwave-assisted method. This microwave approach allowed for even heating, better dispersion, and enhanced surface functionalization compared to traditional techniques. After the nanocomposite synthesis, X-ray diffraction (XRD) was used to assess the crystalline phases and structural integrity of the composite material. Fourier transform infrared spectroscopy (FT-IR) helped identify functional groups and verify that surface modifications were successfully made. Thermogravimetric analysis (TGA) was performed to analyze thermal stability and composition. Scanning electron microscopy (SEM) was employed to investigate surface morphology and particle distribution. The adsorption efficiency of the created nanocomposite for Remazol Red dye was assessed under microwave-assisted conditions. Results: Structural and physicochemical analyses confirmed the successful incorporation of magnetite nanoparticles within the bentonite framework and their functionalization with glutamic acid, which provided numerous active sites for adsorption. The findings indicated fast adsorption kinetics and high removal rates, with nearly total dye elimination achieved in brief contact periods. Discussion: Kinetic analysis suggested that the adsorption process conforms to a pseudo-second-order model, highlighting a predominant chemisorption mechanism. Isotherm analyses aligned well with the Langmuir model, indicating monolayer adsorption on a uniform surface. Thermodynamic analysis verified that the adsorption process is spontaneous and characterized by endothermic behavior. Furthermore, the nanocomposite showed remarkable reusability, consistently delivering high performance throughout several adsorption-desorption cycles. When applied to real water samples, it showcased its practical viability, achieving removal efficiencies greater than 95%. Conclusion: In summary, the microwave-assisted Fe_3O_4@BNT@GA nanocomposite is a promising, environmentally friendly, and effective adsorbent for advanced wastewater remediation applications.

ARTICLE HISTORY

Received: 12 Feb. 2026

Revised: 19 Jul. 2026

Accepted: 11 Sep. 2026

Keywords: Bentonite, Glutamic acid, Remazol red, Magnetite, Microwave, Water remediation.

*Corresponding Author: Dr. Rehab Mansor rehab.mansour@pu

1. Introduction

Water pollution caused by industrial effluents is one of the most pressing environmental concerns worldwide. Among these pollutants, synthetic dyes—particularly azo dyes such as Remazol Red—are widely used in textile, leather, and paper industries (Balasundharam et al., 2026). These dyes are not only aesthetically displeasing but also toxic, carcinogenic, and resistant to biodegradation, making their removal from wastewater a significant challenge. To address the environmental challenges posed by industrial water pollution, researchers have turned to adsorption technologies using eco-friendly and cost-effective materials (Kumar et al., 2026). Natural clay minerals, such as bentonite, have proven to be efficient adsorbents due to their large surface area, ion-exchange capacity, and availability. Bentonite's negatively charged surfaces allow for strong electrostatic interactions with positively charged dye molecules, while its interlayer spaces can accommodate various organic and inorganic species, enhancing adsorption capacity. However, raw bentonite alone may have limitations in adsorption rate and selectivity, which has led to modifications through surface functionalization and composite formation. (Riaz et al, 2015). At the same time, magnetite (Fe_3O_4) nanoparticles provide magnetic separability and high surface reactivity, making them suitable for forming composite materials (Siwi et al., 2026). Moreover, incorporating biomolecules such as glutamic acid can enhance surface functionality by introducing amino and carboxyl groups, which interact effectively with dye molecules (Inbaraj et al, 2011). In recent years, microwave-assisted synthesis has emerged as an efficient and sustainable technique for the preparation of advanced nanocomposites with tailored structural and surface properties (Girdthep et al., 2026). Unlike conventional heating methods that rely on conduction and convection, microwave irradiation interacts directly with polar molecules and conductive components, providing rapid, volumetric heating and uniform temperature distribution (Adhikari et al., 2026). This approach often leads to shorter reaction times, improved particle crystallinity, enhanced dispersion, and higher porosity. When applied to the synthesis of magnetite–bentonite–glutamic acid composites, microwave irradiation enhances the structural integrity of the material and improves the distribution of functional groups on the surface (Hessien et al, 2022). Beyond synthesis, microwave energy can further improve the adsorption performance during water treatment. By increasing molecular mobility, decreasing boundary layer resistance, and accelerating intraparticle diffusion, microwave-assisted adsorption reduces equilibrium time and increases the overall removal efficiency of pollutants (Girdthep et al., 2026). The combination of magnetite, bentonite, and glutamic acid, together with microwave-assisted preparation, leverages synergistic effects that overcome the individual limitations of each component, resulting in a high-performance, magnetically recoverable, and potentially reusable adsorbent (Gabano et al, 2022). Given the urgent need for effective, cost-efficient, and environmentally friendly solutions to industrial dye pollution, the microwave-assisted preparation of magnetite@bentonite@glutamic acid composites presents a promising strategy. This approach not only ensures enhanced adsorption efficiency and selectivity toward dyes like Remazol Red but also provides a feasible pathway toward scalable and sustainable wastewater treatment technologies. Therefore, the present study aims to develop a microwave-assisted Fe_3O_4@BNT@GA nanocomposite and evaluate its efficiency for the removal of Remazol Red dye under microwave-enhanced conditions. The adsorption behavior is systematically investigated through kinetic, isotherm, and thermodynamic analyses, along with reusability and real-sample applications, to assess its potential for sustainable wastewater treatment.

2. Experimental

2.1. Materials and Chemicals

Bentonite clay served as the primary adsorbent material without any additional purification. Iron salts, such as ferric chloride ($FeCl_3 \cdot 6H_2O$) and ferrous sulfate ($FeSO_4 \cdot 7H_2O$), were utilized as precursors for the synthesis of magnetite. Glutamic acid acted as a functionalizing agent to add active surface groups. Sodium hydroxide (NaOH) was employed to adjust the pH and facilitate precipitation. Remazol Red dye was chosen as the model pollutant for the adsorption investigations. All chemicals were of analytical grade and were used as received, without any further processing. Deionized water was employed consistently throughout all experiments.

2.2. Synthesis

2.2.1. Microwave preparation of nanomagnetite (nFe3O4)

Magnetite nanoparticles (Fe_3O_4) were produced using a co-precipitation technique. To summarize, Fe^{3+} and Fe^{2+} salts were dissolved in deionized water while continuously stirring at a microwave oven (approximately 70–80 °C). The molar ratio of Fe^{3+} to Fe^{2+} was kept at 2:1. Following this, NaOH solution was added dropwise until the pH reached around 10, which resulted in the formation of a black precipitate. The mixture was stirred for an additional 30 to 60 minutes to ensure that precipitation was complete (Mahmoud et al, 2021). The resulting Fe_3O_4 nanoparticles were collected using magnetic separation, thoroughly washed multiple times with deionized water and ethanol to eliminate any impurities, and then dried at a microwave oven (about 60 °C).

2.2.2. Preparation of Fe_3O_4@Bentonite Composite

The Fe_3O_4@BNT composite was prepared by dispersing 5 g of bentonite in 20 ml deionized water under vigorous stirring to achieve a homogeneous suspension. The previously synthesized Fe_3O_4 nanoparticles (5 g) were then added to the suspension and mixed thoroughly.

The mixture was subjected to continuous stirring and, and heated in a microwave oven to near dryness to facilitate the deposition of Fe_3O_4 onto the bentonite layers. After sufficient interaction time, the composite was separated, washed repeatedly to remove unbound particles, and dried at 70 °C (Calimli et al, 2020).

2.2.3. Functionalization with Glutamic Acid (Fe_3O_4@BNT@GA)

Surface functionalization was achieved by dispersing the Fe_3O_4@BNT composite in a water solution containing glutamic acid. The mixture was stirred under controlled conditions to facilitate interaction between the functional groups of glutamic acid and the surface of the composite. To improve the efficiency of the functionalization, the suspension underwent microwave irradiation for a brief period. This microwave treatment ensured uniform heating and enhanced the grafting of –COOH and $–NH_2$ groups onto the surface of the composite. Following the treatment, the resulting Fe_3O_4@BNT@GA nanocomposite was magnetically separated, thoroughly washed to eliminate any excess reagents, and dried at 60 °C for future use.

2.3. Characterization Techniques

After the nanocomposite synthesis, X-ray diffraction (XRD) was used to assess the crystalline phases and structural integrity of the composite material. Fourier transform infrared spectroscopy (FT-IR) helped identify functional groups and verify that surface modifications were successfully made. Thermogravimetric analysis (TGA) was performed to analyze thermal stability and composition. Scanning electron microscopy

(SEM) was employed to investigate surface morphology and particle distribution.

2.4. Batch Adsorption Experiments

Batch adsorption experiments were conducted to assess the efficiency of Remazol Red dye removal. A specific amount of nanocomposite was introduced into dye solutions with known concentrations (10, 20, 30 mg/L). The mixture was stirred under controlled conditions, and samples were collected at set time intervals. The influence of different parameters such as pH (ranging from 2 to 10), contact time, adsorbent dosage, and temperature was examined systematically. The pH of the solution was modified using dilute solutions of NaOH or HCl. After the adsorption process, the nanocomposite was separated using magnetic methods, and the remaining dye concentration was analyzed through UV–Vis spectrophotometry at λmax= 541 nm.

2.5. Kinetic, Isotherm, and Thermodynamic Studies

The surface charge properties of the nanocomposite were determined using the pH-drift method to identify the point of zero charge (pH_pzc), which helps explain adsorption behavior at different pH levels. To further understand the adsorption mechanism, several kinetic models—including pseudo-first-order, pseudo-second-order, intraparticle diffusion, and Elovich—were applied. The best-fitting model was identified based on correlation coefficients, providing insight into the rate-controlling steps of the process. Adsorption isotherm studies were also conducted to analyze how dye molecules interact with the adsorbent surface at equilibrium. Models such as Langmuir, Freundlich, Temkin, and Dubinin–Radushkevich were used to interpret the data under optimized conditions across a wide concentration range (10–200 mg/L). Additionally, thermodynamic parameters such as Gibbs free energy (ΔG°), enthalpy (ΔH°), and entropy (ΔS°) were calculated using the Van't Hoff equation to assess the spontaneity and thermal nature of the adsorption process (Lavanya et al., 2026). The reusability of the nanocomposite was evaluated through multiple adsorption–desorption cycles, using acid or base washing for regeneration. Results showed that the material could be reused with minimal efficiency loss. Finally, the applicability of the Fe_3O_4@BNT@GA nanocomposite for the removal of Remazol Red dye from real water samples (industrial wastewater, tap water, and river water) was examined under optimal experimental conditions (pH 7.0, 25 °C, contact time 30 min, and adsorbent dosage 0.05 g). Each sample was spiked with 10 mg L^{-1} of RR dye and treated using the same batch procedure described above. The average results from three independent experiments were used to determine the dye removal efficiency (%R) for each water matrix.

3. Results and discussion

3.1. Characterization of the nanocomposite

The structural properties of the synthesized Fe_3O_4@BNT@GA nanocomposite were investigated using XRD, FT-IR, TGA, and SEM analyses. The XRD pattern in Figure 1 of the synthesized Magnetite @Bentonite @Glutamic Acid nanocomposite displays the characteristic reflections of both magnetite and bentonite. A low-angle diffraction peak appears at $2\theta \approx 3°$, corresponding to the (001) basal plane of bentonite, confirming the preservation of the layered montmorillonite structure after microwave-assisted modification. The major diffraction peaks of magnetite (Fe_3O_4) are clearly observed at approximately 30.2°, 35.5°, and 57.1°, which correspond to the (220),

(311), and (511) planes of the spinel structure, respectively. These reflections confirm the successful formation of magnetite nanoparticles within the composite. A broad hump centered around 26–28° is characteristic of the partially amorphous layered silicate structure of bentonite. The absence of any additional impurity peaks indicates that microwave-assisted synthesis did not introduce unwanted crystalline phases. The noticeable broadening of the magnetite peaks suggests a nanoscale crystallite size and uniform dispersion of magnetite throughout the bentonite matrix. Moreover, surface interaction with glutamic acid contributed to minor peak broadening due to functional binding at the magnetite surface (Gao.J et al,2021).

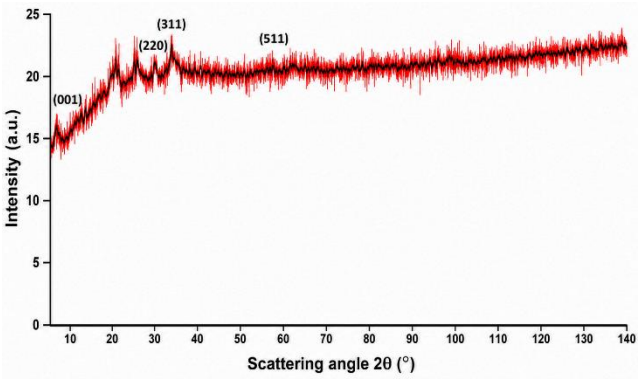

Figure 1: XRD patterns of Fe_3O_4@BNT@GA nanocomposite showing characteristic peaks of magnetite and bentonite phases.

FT-IR analysis further supports successful functionalization. The band at ~1627 cm^{-1} is attributed to C=O and $–COO^-$ stretching vibrations, confirming the incorporation of glutamic acid. Multiple absorption bands in the range of 662–487 cm^{-1} correspond to Fe–O vibrations of magnetite, indicating that the crystalline structure remains intact after microwave processing (Figure 2). The presence of hydroxyl and carboxyl groups enhances the density of active adsorption sites (Khan, M. I. et al, 2021).

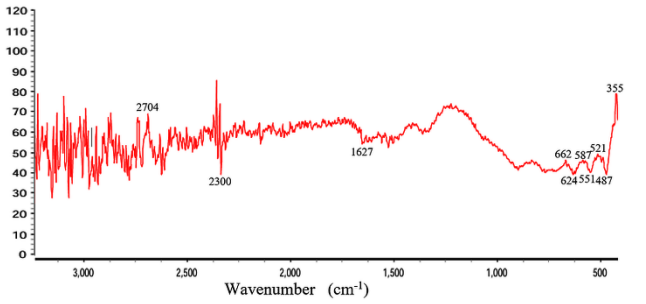

Figure 2: FT-IR spectra confirming functional groups and successful incorporation of glutamic acid into the composite structure.

Thermal analysis showed a multi-step degradation pattern, suggesting the presence of both organic and inorganic elements. The first weight loss is linked to the removal of moisture, which is then succeeded by the breakdown of organic materials and the stabilization of inorganic phases (Figure 3). After heating to approximately 780 °C, a residual mass of about 55–60 mg remains, indicating the presence of thermally stable inorganic constituents or ash that do not undergo further decomposition under the applied conditions. The considerable residual mass indicates that thermally stable mineral components are predominant. This residual mass confirms the incorporation of inorganic components within the sample matrix. The derivative thermogravimetric (DTG) curve exhibits distinct peaks at temperatures corresponding precisely to each weight-loss stage identified in the TGA profile. The position of each DTG peak represents the temperature at which the rate of decomposition is maximal, while the peak intensity reflects the magnitude of the corresponding degradation event. In addition, the differential scanning calorimetry (DSC) curve provides further insight into the thermal transitions of the sample. Endothermic events observed in the range of 100–200 °C are associated with moisture loss, solvent evaporation, or dehydration processes. In contrast, exothermic peaks appearing between 250 and 450 °C correspond to decomposition reactions, oxidative processes, and partial combustion of the organic components (Rathod, V. K. et al, 2021)

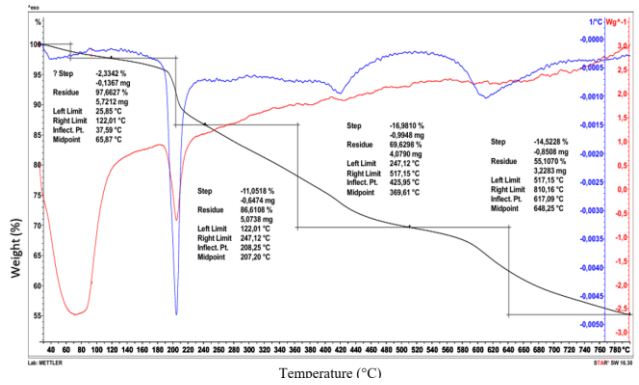

Figure 3: TGA/DTG thermograms illustrating thermal stability and multi-step decomposition behavior of the nanocomposite.

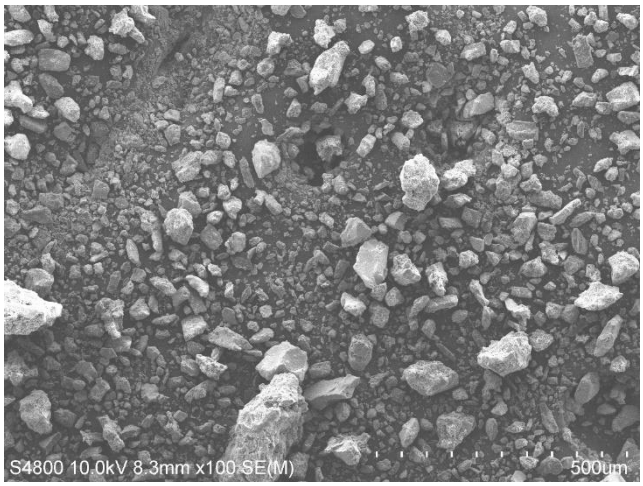

Figure 4: SEM image showing porous morphology and heterogeneous surface structure of Fe_3O_4@BNT@GA.

Figure 4 displays the SEM micrograph of the synthesized Magnetite–Bentonite–Glutamic Acid (MBG) nanocomposite. The image reveals a heterogeneous morphology characterized by irregularly shaped particles of various sizes distributed unevenly across the surface. The composite exhibits a rough and porous structure composed of micro- to submicron-sized granules. From the scale bar (500 µm), the estimated particle size range is approximately 10–80 µm, with some larger agglomerated clusters exceeding 100 µm. These aggregates result from the magnetic dipole–dipole interactions among Fe_3O_4 nanoparticles, leading to partial clustering, which is a common phenomenon in magnetite-based composites. The smaller particles appear to fill the voids among the larger aggregates, forming a complex and multi-layered texture that increases surface heterogeneity. The roughness and irregular surface topology observed in the image confirm the successful deposition and integration of magnetite nanoparticles within the bentonite matrix. This morphology enhances the specific surface area and pore accessibility, both of which are crucial for adsorption efficiency. The presence of pores and cavities between aggregated particles indicates potential adsorption sites for dye molecules, contributing to a higher adsorption capacity of the MBG nanocomposite. Furthermore, the incorporation of glutamic acid appears to have played a significant role in stabilizing the magnetite nanoparticles and improving the interfacial adhesion between the organic and inorganic components. The amino and carboxyl groups of glutamic acid likely interacted with Fe and Si–O groups of magnetite and bentonite, respectively, thereby promoting a more cohesive and functional hybrid structure. This organic modification prevents excessive aggregation and helps maintain a porous morphology suitable for microwave-assisted adsorption applications (El-Maghraby, M. S. et al, 2021).

3.2. Dye adsorption study

3.2.1. Effect of pH and Surface Charge Behavior

Figure (5.a) illustrates the effect of the initial pH of the solution on the removal efficiency (%) of the studied dye at two initial concentrations, 15 ppm and 30 ppm, over a pH range of 2.0–10.0. The effectiveness of adsorption was heavily influenced by the pH of the solution, which affects both the charge of the adsorbent surface and the form of the dye. The highest removal efficiency, around 90–93%, was recorded at pH levels between 6 and 7. At lower pH levels, an abundance of H^+ ions compete with dye molecules for adsorption sites, leading to a decline in efficiency. On the other hand, at higher pH levels (above 7), the electrostatic repulsion between negatively charged surface sites and dye molecules results in decreased adsorption.

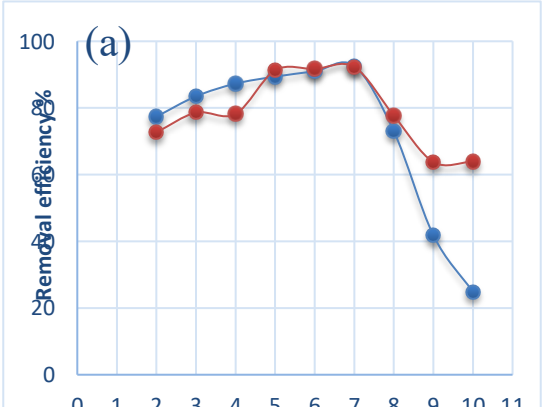

Figure (5.b) shows how ΔpH (pH_final – pH_initial) changes with the initial pH of the solution to determine the point of zero charge (pHpzc) of the prepared adsorbent. The point of zero charge ($pH_pzc \approx 5.0$) indicates that the surface carries a positive charge below this threshold and a negative charge above it. The increased adsorption observed close to neutral pH levels implies that both electrostatic interactions and surface functional groups work together to determine the adsorption process. At pH values below pHpzc, excess H^+ ions or electrostatic repulsion can reduce adsorption performance (El-Shafey, E. I.et al, 2021).

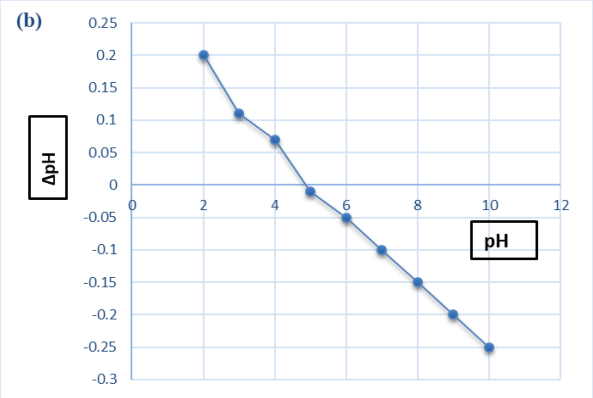

Figure 5: (a) Effect of solution pH on dye removal efficiency; (b) determination of point of zero charge (pH_pzc) at 25 °C.

3.2.2. Effect of Contact Time and Adsorption Kinetics

Figure (6. a) demonstrates the effect of contact time on the removal efficiency of Remazol Red using the Magnetite@Bentonite@Glutamic Acid composite at initial concentrations of 15 ppm and 30 ppm. In both cases, adsorption occurs rapidly during the first 15 minutes due to the availability of abundant active sites on the adsorbent surface. At 15 ppm, removal efficiency quickly reaches about 88% and gradually approaches nearly 100% within 40–50 minutes. At 30 ppm, the efficiency initially rises to around 78% and stabilizes near 95% after approximately 40 minutes. Beyond this time, minimal changes indicate that equilibrium has been reached. The slower initial rate at higher concentration is attributed to the need for more time to saturate the adsorbent surface, although both concentrations follow the same general trend of fast initial adsorption followed by a slower approach to equilibrium. Figure (6. b) evaluates the pseudo-first-order kinetic model using plots of ln ($q_e - q_t$) versus time. The relatively low correlation coefficients ($R^2 = 0.8323$ for 15 ppm and 0.7727 for 30 ppm) indicate poor agreement with this model. This suggests that the adsorption process is not governed by simple physisorption, where adsorption depends only on the availability of vacant sites. In contrast, Figure (6. c) shows that the pseudo-second-order model provides an excellent fit, with very high R^2 values (0.9999 for 15 ppm and 0.9995 for 30 ppm). This strong correlation, along with the close agreement between calculated and experimental adsorption capacities, confirms that chemisorption is the dominant mechanism. This implies that adsorption involves chemical interactions such as electron sharing or exchange between the dye molecules and the composite surface. Figure (6. d) presents the intra-particle diffusion model (q_t vs. $t^{1/2}$). The plots exhibit multi-linearity and do not pass through the origin, with moderate R^2 values (0.837 and 0.8231). This indicates that intra-particle diffusion is involved but is not the sole rate-controlling step. Instead, adsorption proceeds in multiple stages, beginning with rapid surface adsorption followed by slower diffusion into the pores. Similarly, Figure (6. e), which plots q_t versus ln t, confirms that intra particle diffusion contributes partially to the adsorption process. The plots show moderate linearity ($R^2 \approx 0.92$) but do not pass through the origin, indicating that other mechanisms, such as boundary layer diffusion, are also involved. The influence of pore diffusion becomes slightly more significant at higher dye concentrations. Figure (6. f)

illustrates the Avrami kinetic model, which shows good linearity with relatively high R^2 values (0.9432 and 0.9249). This suggests that adsorption follows complex, multi-step pathways. The similar Avrami exponents for both concentrations indicate a consistent mechanism and surface heterogeneity, while positive intercepts suggest cooperative interactions during adsorption. Overall, comparison of all models (Figures 6b–e and Table 1) shows that the pseudo-second-order model best describes the adsorption kinetics. The high correlation coefficients and agreement between calculated and experimental equilibrium capacities confirm that chemisorption is the dominant mechanism governing the removal of Remazol Red by the composite.

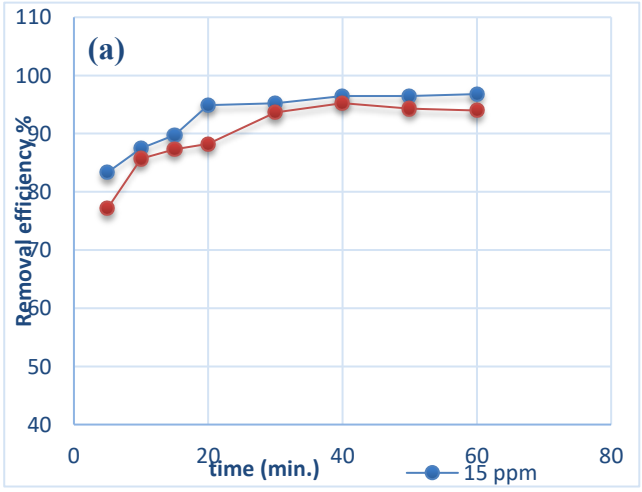

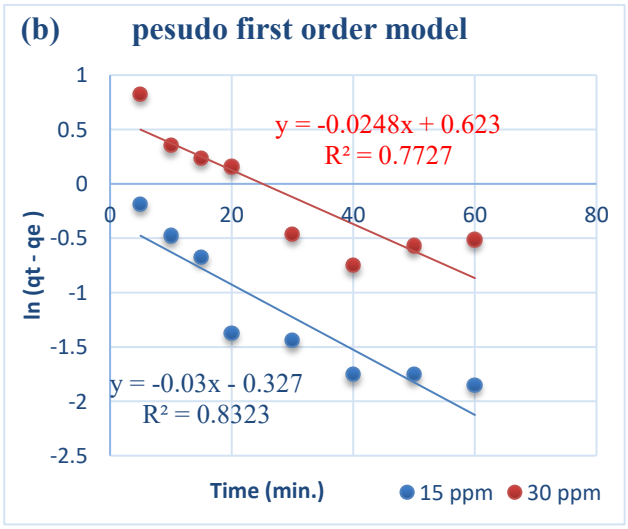

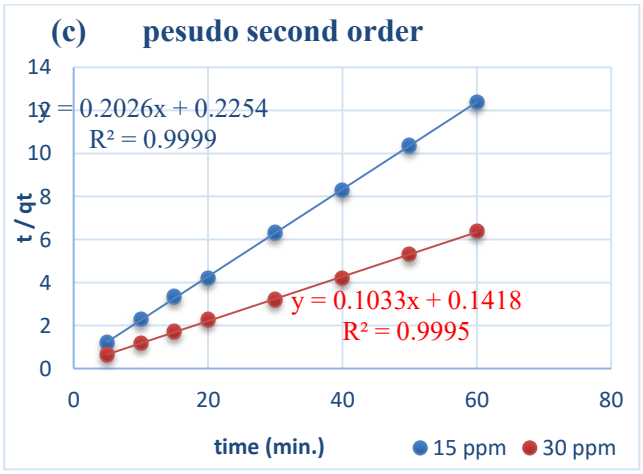

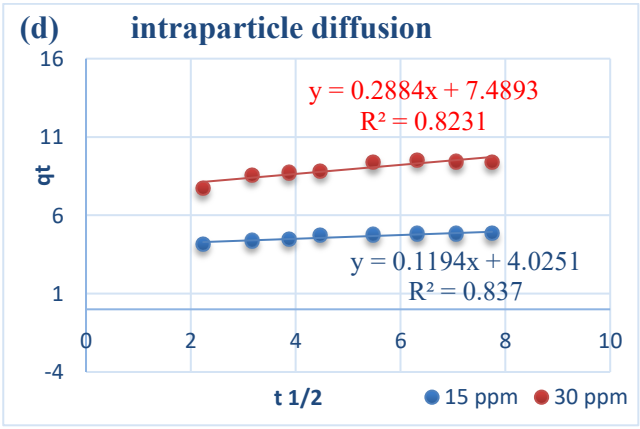

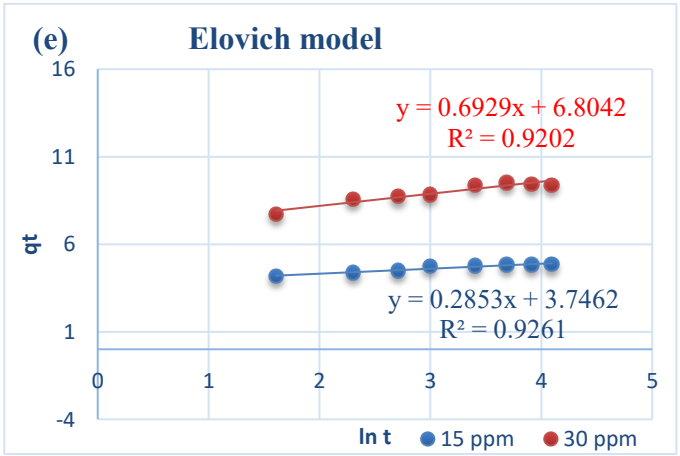

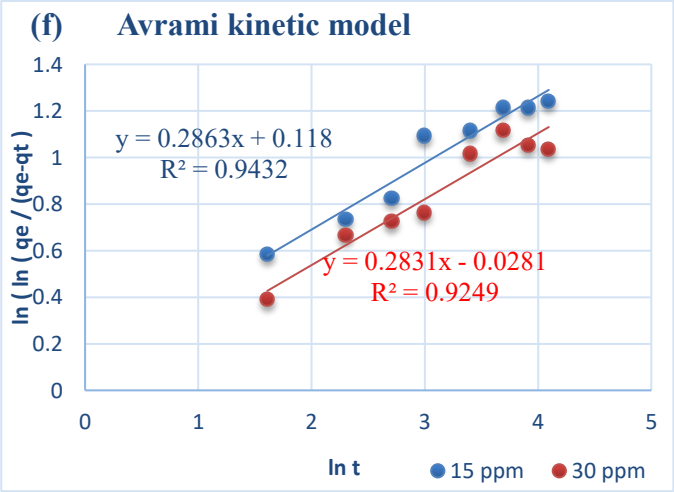

Figure 6: (a) The effect of contact time on the removal efficiency (R%) of Magnetite @Bentonite @Glutamic Acid, (b) Pseudo-first order, (c) Pseudo-second order, (d) Intra-particle diffusion, (e) Elovich kinetic models, and (f) Avrami kinetic models, at 25 °C.

Table 1: Equations of kinetic models and their parameters for the adsorptive removal of Magnetite @ Bentonite @ Glutamic Acid

Kinetic Model	**Equation**	**Plot**	**Kinetic Parameter**	**RRD 15 ppm**	**RRD 30 ppm**
Pseudo-First Order	$Ln\ (q_e - q_t) = Ln\ (q_e) - k_1 t$	$ln\ (q_e - q_t)$ versus time (t), q_e and q_t are the sorption capacity at equilibrium and at time t (min), respectively, k_1 is the first order rate constant	q_e (mg/g) (calc)	0.72108374	1.8645132
			K_1 (min^{-1})	0.03	0.0248
			R^2	0.8323	0.7727
Pseudo-Second Order	$t/q_t = 1/k_2 q_e^2 + t/q_e$	t/q_t versus time (t), K_2 is the second order rate constant	q_e (mg/g) (exp)	4.9358342	9.43
			q_e (mg/g) (calc)	4.8233333	9.6805421
			K_2 (g/mg min)	0.190727	0.07930496
			R^2	0.9999	0.9995
Intra-particle Diffusion	$q_t = k_{id}\ t^{0.5} + C$	q_t versus ($t^{0.5}$), C is the thickness of the adsorption layer, K_{id} is the intra-particle order rate constant	K_{id} (mg/g $min^{0.5}$)	0.1194	0.2884
			C	4.0251	7.4893
			R^2	0.837	0.8321
Elovich	$q_t = 1/\beta\ Ln(\alpha\beta) + 1/\beta\ Ln\ (t)$	q_t versus ln t, α is the initial adsorption rate, β is related to the extent of surface coverage and the activation energy for the chemisorption process	α (mg/g min)	143749.08	12746.574
			β (mg/g)	3.505082	1.44321
			R^2	0.9432	0.9202

3.2.3. Effect of Initial Dye Concentration and Adsorption Isotherms

The initial concentration of Remazol Red significantly influences the adsorption efficiency of the Magnetite@Bentonite@Glutamic Acid (MBG) composite. At low dye concentrations, removal efficiency is high due to the abundance of available active sites on the adsorbent surface. Maximum removal occurs around 10 mg/L, where most adsorption sites are effectively occupied Figure (7. a). However, as the dye concentration increases beyond this level, efficiency declines. This decrease is attributed to the saturation of active sites and the aggregation of dye molecules, which reduces their interaction with the adsorbent. Thus, higher dye concentrations can exceed the adsorption capacity of the MBG composite. Isotherm analysis provides further insight into the adsorption mechanism. The Langmuir model shows an excellent fit (R^2 = 0.9682), indicating monolayer adsorption on a homogeneous surface with identical binding sites Figure (7. b). This suggests that the MBG composite offers uniform adsorption sites and that dye molecules form a single layer at equilibrium, making the Langmuir model the most appropriate for describing the system. The Freundlich model, which assumes heterogeneous surfaces and multilayer adsorption, also shows good linearity (R^2 = 0.9977) but is less representative of the system compared to Langmuir Figure (7. c). Although it indicates favorable adsorption, it does not fully capture the actual mechanism. The Temkin model Figure (7. d) yields a moderate correlation (R^2 = 0.8251), suggesting that adsorbate–adsorbent interactions exist but are not the dominant factor controlling adsorption. The Dubinin–Radushkevich (D–R) model shows the weakest fit (R^2 = 0.6199), indicating poor applicability Figure (7. e). Its results suggest that the adsorption process is mainly physical rather than chemical. Overall, the analysis confirms that the Langmuir model best describes the adsorption behavior, highlighting monolayer adsorption on a homogeneous MBG surface with strong adsorption performance.

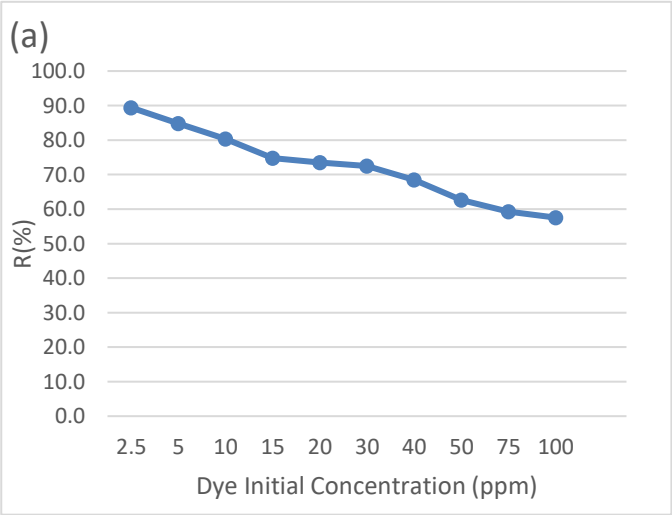

(b)

(c)

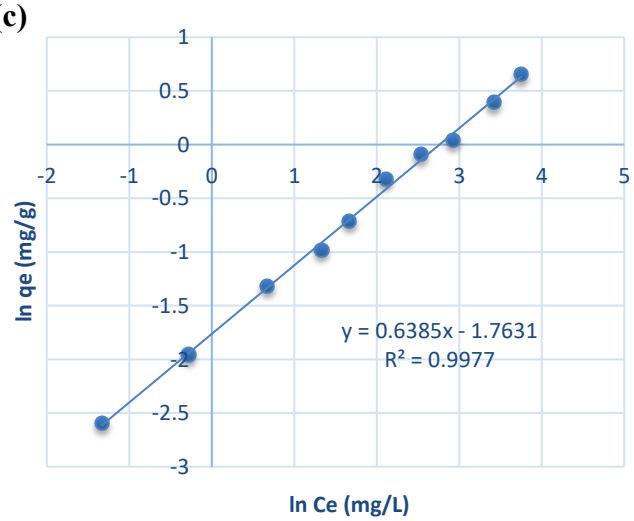

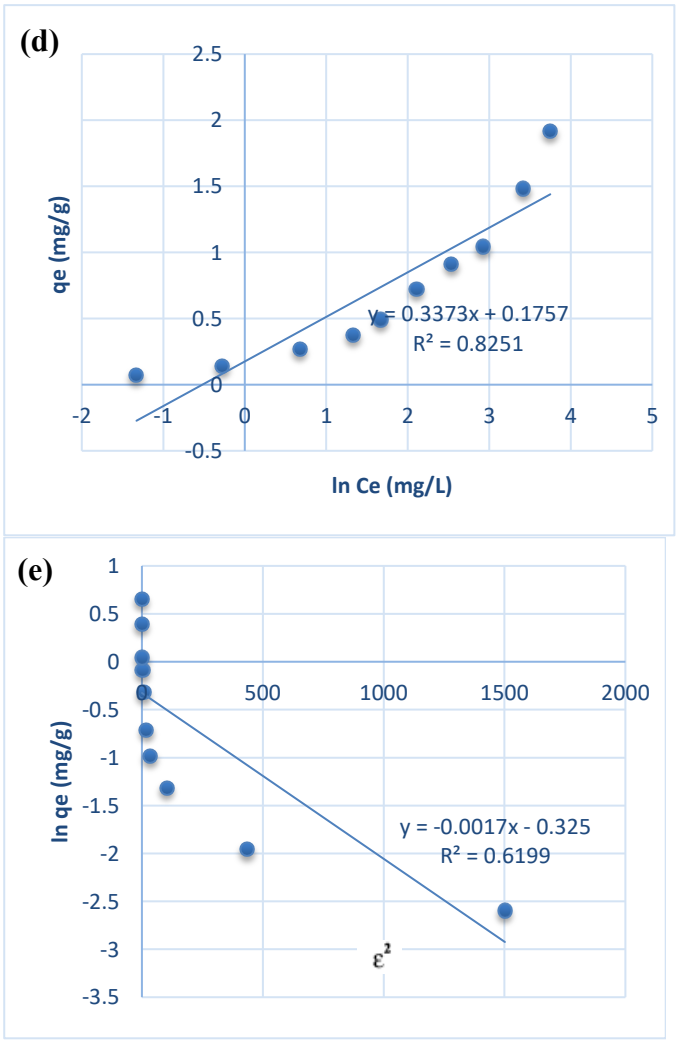

Figure 7: Figure 7. (a) The effect of initial Magnetite @Bentonite @Glutamic Acid concentration on the removal efficiency (R%), (b) Langmiur, (c) Freundlich, (d) Temkin, and (e) isotherm models for MBG adsorption onto the at 25 °C.

The adsorption behavior of Remazol Red dye was analyzed using several isotherm models (Table 2 and Figure 7). The experimental data showed a good fit with the Langmuir model ($R^2 = 0.9682$), indicating monolayer adsorption, with a maximum capacity of 0.839 mg/g and favorable conditions at pH 7. The separation factor (RL) values between 0 and 1 confirmed the feasibility of adsorption. The Freundlich model provided an even better fit ($R^2 = 0.9977$), suggesting heterogeneous surface adsorption, with an adsorption intensity (n = 1.566) indicating favorable uptake and a high adsorption capacity (Kf = 0.172 L/mg). In contrast, the Temkin and Dubinin–Radushkevich models showed low correlation coefficients, indicating they poorly describe the adsorption process (Al-Shamrani, A.et al, 2023).

Table 2:Linear equations and their parameters for different adsorption isotherm models for the 15 ppm and 30 ppm adsorptive removal by the Magnetite @ Bentonite @ Glutamic Acid

Isotherm Model	**Linear Equation**	**Linear Plot**	**Isotherm Parameter**	**RRD**
Langmuir	$C_e/q_e=1/q_{max}K_L+C_e/q_{max}$	1/q_e versus 1/C_e, slope = $1/q_m$, and intercept =$1/(K_L\ q_{max})$; K_L is the Langmiur constant, q_{max} is the maximum adsorption capacity, $R_L=\frac{1}{1+K_LC_o}$, C_o is the initial concentration of U(IV) ions in mg/L	q_{max} (mg/g)	0.838789743
			K_L(L/mg)	0.350625472
			R_L	(0.02773 - 0.487359)
			R^2	0.9682
Freundlich	$\ln(q_e)=\ln(K_F)+1/n\ln(C_e)$	Ln q_e versus ln C_e, slope = 1/n, and intercept = ln K_F; K_F is the Freunlish constant related to the affinity of the adsorbate to the binding sites of the adsorbent, n is the intensity of the adsorbent	n	1.566170713
			K_F (L/mg)	0.171512351
			R^2	0.9977
Temkin	$q_e=(RT/b_T)\ln(a_T)+(RT/b_T)\ln(c_e)$	q_e versus ln C_e, slope = B = RT/b_T, and intercept = Bln a_T; a_T is Temkin isotherm equilibrium binding constant corresponding to the maximum binding energy, b_T is the Temkin isotherm equilibrium binding constant related to the heat of adsorption and/or the adsorption bonding energy, R is the gas constant = 8.314×10^{-3} kJ mol^{-1} K^{-1}, T is the absolute temperature in K	a_T (L/mg)	1.683555
			b_T(KJ/mol)	7.345486384
			B	0.337291756
			R^2	0.8251
Dubinin Radushkevich (D–R)	$\ln(q_e)=\ln(q_s)-(K_{ad}\varepsilon^2)$	Ln q_e versus ε^2, slope = K_{ad}, and intercept = Ln (q_s); ε is the *polanyi* potential (ε = RT ln (1+(1/C_e)), q_s is the theoretical saturation capacity, K_{ad} is the D-R isotherm constant, $E_s=\frac{1}{\sqrt{2K_{ad}}}$	q_{max} (mg/g)	0.722527354
			K_{ad} (mol^2/J^2)	17
			E_s(KJ/mol)	0.171498
			R^2	0.6199

3.2.4. Effect of Adsorbent Dosage and Temperature

The adsorption performance of MBG is strongly influenced by sorbent mass, temperature, and thermodynamic behavior. Increasing the sorbent mass from 5 mg to 40 mg significantly enhances the removal efficiency (R%) for both 15 ppm and 30 ppm dye concentrations Figure (8. a). At low dosages, the limited number of active adsorption sites restricts dye uptake, resulting in lower removal efficiency. As the sorbent mass increases, more active sites become available, strengthening interactions between the dye and the sorbent. This leads to a sharp improvement in R%, especially between 5 mg and 20 mg, with the effect being more noticeable at 15 ppm. However, beyond 40 mg, the removal efficiency approaches a plateau, indicating that adsorption equilibrium is nearly reached. At higher dosages, particle agglomeration and surface crowding may reduce the effective surface area and block active sites, limiting further improvement. Therefore, 40 mg is identified as the optimal sorbent mass. Thermodynamic analysis using van't Hoff plots shows a linear relationship between ln Kd and 1/T for both concentrations, indicating predictable behavior Figure (8. b). The 30 ppm system demonstrates a stronger linear fit ($R^2 \approx 0.8506$), suggesting more stable thermodynamic performance, while the 15-ppm system shows greater variability ($R^2 \approx 0.725$). The increase of Kd with temperature indicates that the adsorption process is overall endothermic, meaning it is enhanced by higher temperatures. Additionally, the 15-ppm system appears more sensitive to temperature changes. Temperature also plays a key role in adsorption efficiency. As temperature increases from 285 K to 330 K, R% rises steadily for both concentrations Figure (8. c). Higher temperatures increase molecular motion, improving collision frequency and diffusion of dye molecules into MBG pores. This effect is more pronounced at 30 ppm, where higher dye concentration benefits more from enhanced mass transfer. Overall, adsorption is thermally promoted and diffusion-controlled.

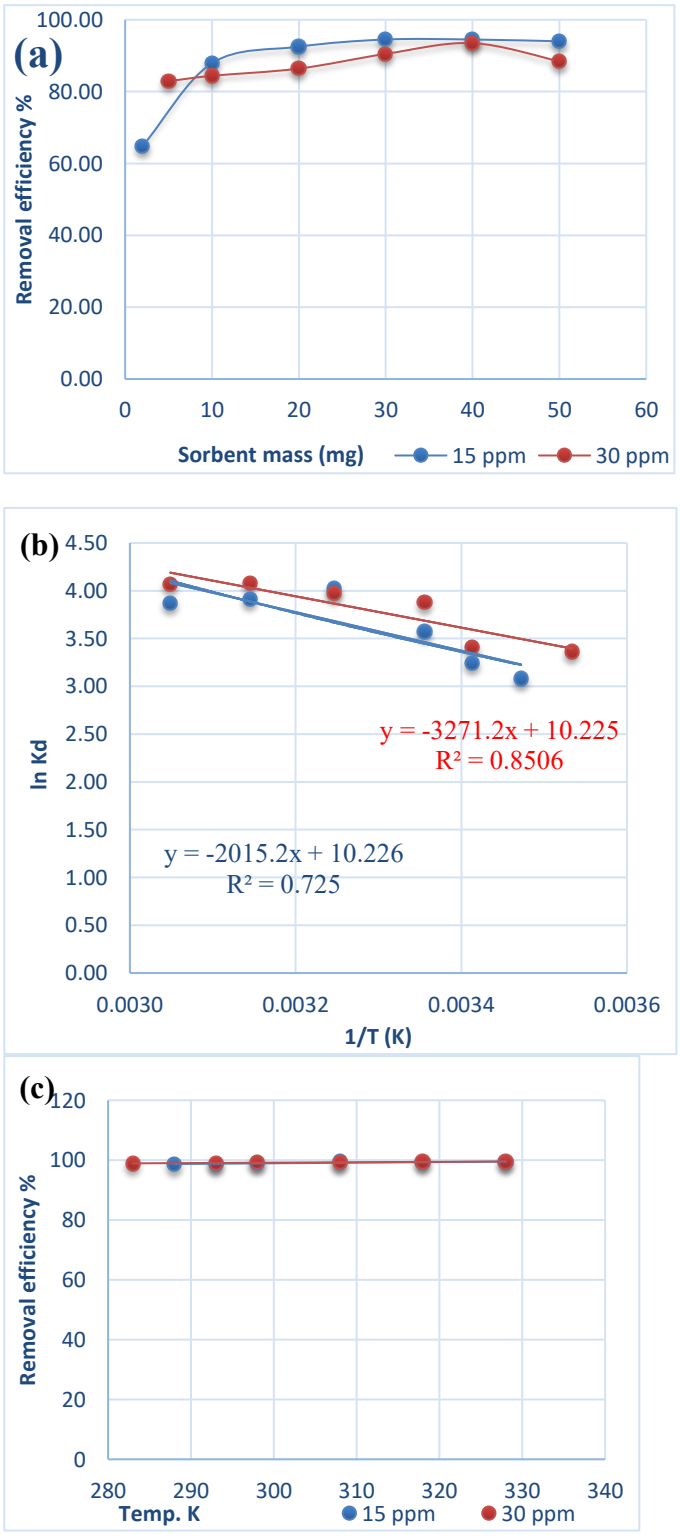

Figure 8: (a) The effect of the MBG mass dosage, (b) the effect of reaction temperature on the removal efficiency (R%) of MBG dye pollutants, (c) Vant Hoff plot for the adsorption of MBG.

Data collected from the experiments above, pertaining to the effect of temperature on the adsorption reaction were

employed to calculate the thermodynamic parameters of this reaction. These include Gibbs free energy (ΔG°, KJmol-1),

Table 3: Standard thermodynamic parameters for the adsorption of 15 ppm and 30 ppm onto the Magnetite @ Bentonite @ Glutamic Acid at different reaction temperatures.

Dye initial concentration (ppm)	**Temperature (K)**	**LnK_d (L/g)**	**Adsorption Thermodynaic Paramters**			**R^2**
			-ΔG° (KJmol^{-1})	**ΔH° (KJmol^{-1})**	**ΔS° (Jmol^{-1}K^{-1})**	
15 ppm	**283**	3.08	7244.90	16.7543728	85.018964	0.725
	293	3.24	7893.61			
	298	3.57	8848.24			
	308	4.02	10296.96			
	318	3.91	10337.77			
	328	3.87	10553.47			
30 ppm	**283**	3.36	7911.56	27.1967568	85.01065	0.8506
	293	3.41	8296.90			
	298	3.88	9603.44			
	308	3.97	10176.82			
	318	4.08	10779.38			
	328	4.07	11088.85			

standard enthalpy change (ΔH°, KJmol-1), standard entropy change (ΔS° , Jmol-1K-1), and the adsorption equilibrium constant (Kd, L/g) (Ahamad, Z. et al, 2024). These parameters are considered important in deducing the nature of the adsorption reaction and degree of spontaneity. The slope of the linear Vant Hoff's plot (ln Kd vs 1/T, Fig (8.a)) is employed to calculate the value of ΔH°. The intercept in this plot is used to calculate the value of ΔS° . The calculated results of all the investigated thermodynamic parameters, along with the linear correlation coefficient values (R2) are provided in Table 3. From Figure (8.a), it is evident that all points over the experimental temperature range are located on a straight line. This implies that the experimental adsorption data were well fitted with the thermodynamic relation based on the high values of linear correlation coefficients, where R2 = 0.725 for 15 ppm and 0.8506 for 30 ppm. Table 3 shows that the ΔG° values were in the range from -7244.90 to -10553.47 KJmol-1 for 15 ppm and from -7911.56 to -11088.85 KJmol-1 for 30 ppm in the reaction temperature range 283–328 K.

3.3. Regeneration and Reusability of MBG

The reusability of adsorbents is a critical parameter for their practical application, as it directly influences both cost-effectiveness and sustainability. In the case of MBG, strong interactions between the support matrix (Magnetite @ Bentonite) and glutamic acid, combined with its magnetic properties and enhanced nanocomposite stability, enable efficient repeated use in adsorption and magnetic separation processes. The reusability of MBG was assessed over five consecutive adsorption–desorption cycles using Remazol Red as the target pollutant. After each cycle, the adsorbent was recovered with an external magnet, thoroughly washed with phosphate-buffered saline (PBS, 0.1 M, pH 7.4), dried at room temperature, and reused in the subsequent cycle. The removal efficiency (R%) was normalized relative to the first cycle. Experimental results showed that MBG achieved a removal efficiency of 99.37% during the first cycle. After five cycles, the efficiency slightly decreased to 97.42%, indicating only a minimal loss in performance. This excellent recyclability can be attributed to the strong covalent and non-covalent interactions between the support matrix and the immobilized functional groups, which help preserve structural integrity during repeated use. The slight reduction in removal efficiency over multiple cycles may be explained by several factors, including: (1) incomplete desorption of dye molecules from MBG pores; (2) particle aggregation during magnetic separation; (3) partial blockage of active adsorption sites; (4) gradual leaching or denaturation of functional groups; and (5) minor material loss during handling. Despite these limitations, MBG retained a high adsorption capacity after repeated regeneration cycles, demonstrating its strong potential as a sustainable and efficient adsorbent for the removal of cationic dyes from wastewater.

3.4. Remediation of Real Water Samples

The practical use of the synthesized MBG (Magnetite @ Bentonite @ Glutamic Acid) bio-nanocomposite was further assessed through adsorption tests using actual water samples. This evaluation is crucial to confirm its effectiveness beyond controlled lab settings and to establish its potential for real-world wastewater treatment applications. Batch equilibrium experiments were performed on various water samples, including tap water, industrial wastewater, and seawater, each containing 10 mg/L of Remazol Red. The adsorption process was conducted under optimized conditions established from laboratory-scale studies to ensure consistent and comparable results. The removal efficiencies achieved were 95.09% for tap water, 95.47% for industrial wastewater, and 96.24% for seawater. The consistently high removal rates across all tested samples indicate that the presence of competing ions and background materials in real water systems did not notably impede the adsorption capabilities of the MBG. This points to a strong interaction between the bio-nanocomposite and the dye molecules, likely due to the synergistic effects of magnetite, bentonite, and glutamic acid functional groups. Interestingly, the marginally greater removal efficiency seen in seawater might be linked to ionic strength effects that improve adsorption interactions. However, additional research is needed to fully clarify this phenomenon. In general, the results demonstrate that MBG retains remarkable adsorption capacity even in challenging environmental conditions. These findings emphasize the durability and efficacy of the bio-nanocomposite developed, reinforcing its potential as a quick and effective adsorbent for eliminating harmful dyes from various water sources. The strong performance noted in actual samples highlights its potential for practical use in wastewater treatment systems.

4. Conclusion

A novel Fe_3O_4@BNT@GA nanocomposite, which can be magnetically recovered, was successfully created using a quick microwave-assisted method. This technique facilitated the effective combination of inorganic and organic components, leading to a highly

functionalized and porous structure. The nanocomposite showed remarkable adsorption capabilities for Remazol Red, achieving rapid kinetics and impressive removal efficiency. The adsorption process conformed to pseudo-second-order kinetics and was best represented by the Langmuir isotherm, suggesting the occurrence of monolayer chemisorption. Thermodynamic evaluations indicated that the process is both spontaneous and endothermic, with improved performance at higher temperatures. Additionally, the material exhibited exceptional reusability and high efficiency in actual water systems. In summary, this research underscores the potential of microwave-assisted synthesis for creating advanced, sustainable nanocomposites suitable for wastewater treatment, providing a scalable and eco-friendly approach for dye removal.

Acknowledgment:

The authors would like to express their sincere gratitude to Rojava University and Institute of science and technology for providing access to the laboratory facilities and resources essential for conducting this research. We sincerely acknowledge NGO Emmaus Jokioinen for its valuable technical support in conducting thermogravimetric analysis (TGA) and scanning electron microscopy (SEM) of the synthesized nanocomposite, which significantly contributed to this study.

Authors' contribution:

This paper is extracted from a Master thesis, for which Haidar Saify, Mohamed E.Mahmoud and Rehab M .El-Sharkawy were Supervisors of the project, chief investigators, and responsible for the data analysis. Methodology and first draft of the manuscript were done by Maher.

Funding:

We confirm that this work did not receive any grant from funding agencies in the commercial, public sectors.

Declarations

Conflict of interest

The authors declare that they have no known competing interests.

Data availability

Data generated or analyzed during this project are provided in full within the published article

Reference

1. Ahamad, Z., & Nasar, A. (2024). Polypyrrole-decorated bentonite magnetic nanocomposite: A green approach for adsorption of anionic methyl orange and cationic crystal violet dyes from contaminated water. Environmental Research,247, 118193.
2. Adhikari, Ashok, Francisco J. Cano, Rocío Magdalena Sánchez-Albores, Javier Aguila-Rosas, María de la Luz Olvera Amador, and Odín Reyes-Vallejo. "Microwave-Assisted Synthesis of Nanomaterials: Parameters, Advantages, and Challenges for Energy and Environmental Applications." In Handbook of Nanomaterials and Nanocomposites for Energy and Environmental Applications, pp. 1-36. Cham: Springer Nature Switzerland, 2026.
3. Al-Shamrani, A., & Khan, M. R. (2023). Adsorption performance of zeolite for the removal of Congo Red dye: Factorial design

experiments, kinetic, and equilibrium studies. Separations, 10(1), 57.

4. Balasundharam, Nishaa, and Karthikeyan Ramalingam. "Eco-friendly remediation of reactive azo dye-laden wastewater via Lactobacillus casei immobilized on porous clay: mechanistic and phytotoxicity insights." Biodegradation 37, no. 1 (2026): 5.
5. M.E. Mahmoud, R.M. El-Sharkawy, G.A.A. Ibrahim, Promoted adsorptive removal of chromium(VI) ions from water by a green-synthesized hybrid magnetic nanocomposite (NFe3O4Starch-Glu-NFe3O4ED), RSC Adv. 11 (2021) 14829.
6. M.H. Calimli, M.S. Nas, H. Burhan, S.D. Mustafov, Ö. Demirbas, F. Sen, Preparation, characterization and adsorption kinetics of methylene blue dye in reduced-graphene oxide supported nanoadsorbents, J. Mol. Liq. 209 (2020).
7. El-Shafey, E. I. (2021). Surface charge studies of modified bentonite and their impact on dye adsorption. Applied Clay Science, 205, 106062.
8. Rathod, V. K., & Pandit, A. (2021). Thermal stability assessment of polymer magnetite nanocomposites using thermogravimetric techniques. Polymer Degradation and Stability, 193, 109712.
9. Riaz, M., Khan, S., & Iqbal, M. (2015). Microwave-induced catalytic degradation of a textile dye using bentonite-poly(o-toluidine) nanohybrid. RSC Advances, 5, 78945–78953.
10. El-Maghraby, M. S., & El-Sheikh, S. M. (2021). SEM–EDX analysis of functionalized bentonite-based adsorbents. Journal of Environmental Chemical Engineering, 9, 105782.
11. Gabano, E. (2022). Microwave-assisted green synthesis overview. Molecules, 27, 5432.
12. Gao, J., Fan, H., & Liu, X. (2021). Crystalline phase evaluation of bentonite–magnetite hybrid adsorbents by XRD and Rietveld refinement. CeramicsInternational, 47, 21452–21460.
13. Girdthep, Sutinee, Soontorn Suvokhiaw, Siirat Choosakoonkriang, Gulanat Chanachinrat, and Cheewita Suwanchawalit. "Microwave-Assisted Synthesis of Boron and Nitrogen Co-Doped Carbon Dots Immobilized on SiO2 Nanoparticles for High-Resolution Latent Fingerprint Detection." Optical Materials (2026): 117919.
14. Khan, M. I., & Shah, Z. (2021). Functional group characterization of amino-acid-modified magnetic adsorbents using FTIR. Spectrochimica Acta Part A, 258, 119807.
15. Kumar, Kuldeep, Ravi Kumar, and Naveen Thakur. "Biogenic Nanocomposites for the Removal of Dyes and Micropollutants from Wastewater." In Nanotechnology in Environmental Science and Healthcare, pp. 39-53. Singapore: Springer Nature Singapore, 2026.
16. Lavanya, M., and S. Karthick Raja Namasivayam. "Nanoscale zinc oxide (ZnO NPs)–alginate–PEG–activated carbon nanocomposite for efficient Cr (VI) removal from electroplating wastewater: adsorption isotherms and eco-toxicity evaluation." Journal of Chemical Technology & Biotechnology 101, no. 4 (2026): 886-903.

17. Hessien, M. M. H. C. (2022). Methylene blue dye adsorption on iron oxide-hydrochar composite synthesized via a facile microwave-assisted hydrothermal carbonization of pomegranate peels' waste. Molecules, 27, 4123.
18. Inbaraj, B. S., Chen, B. H., & Lin, F. H. (2011). Dye adsorption characteristics of magnetite nanoparticles coated with a biopolymer poly(γ-glutamic acid). Bioresource Technology, 102, 8524–8531.
19. Siwi, Dewinta Yuka, Anugrah Ricky Wijaya, Neena Zakia, and Nor Kartini Abu Bakar. "Synthesis, characterization, and application of Fe_3O_4/PEG/HAp nanocomposite as an adsorbent for Pb (II)." In E3S Web of Conferences, vol. 695, p. 02008. EDP Sciences, 2026.